JACS
JOURNAL OF THE AMERICAN CHEMICAL SOCIETY

ARTICLE

pubs.acs.org/JACS

Linear- and Angular-Shaped Naphthodithiophenes: Selective Synthesis, Properties, and Application to Organic Field-Effect Transistors

Shoji Shinamura,[†] Itaru Osaka,[†] Eigo Miyazaki,[†] Akiko Nakao,[‡] Masakazu Yamagishi,[§] Jun Takeya,[§] and Kazuo Takimiya*[,†,∥]

[†]Department of Applied Chemistry, Graduate School of Engineering, Hiroshima University, Higashi-Hiroshima 739-8527, Japan

[‡]High Energy Accelerator Research Organization (KEK), 1-1 Oho, Tsukuba, Ibaraki 305-0801 Japan

[§]ISIR, Osaka University, Ibaraki 567-0047, Japan

[∥]Institute for Advanced Materials Research, Hiroshima University, Higashi-Hiroshima 739-8530, Japan

Supporting Information

ABSTRACT: A straightforward synthetic approach that exploits linear- and angular-shaped naphthodithiophenes (NDTs) being potential as new core structures for organic semiconductors is described. The newly established synthetic procedure involves two important steps; one is the chemoselective Sonogashira coupling reaction on the trifluoromethanesulfonyloxy site over the bromine site enabling selective formation of *o*-bromoethynylbenzene substructures on the naphthalene core, and the other is a facile ring closing reaction of fused-thiophene rings from the *o*-bromoethynylbenzene substructures. As a result, three isomeric NDTs, naphtho[2,3-*b*:6,7-*b*′]dithiophene, naphtho[2,3-*b*:7,6-*b*′]dithiophenes, and naphtho[2,1-*b*:6,5-*b*′]dithiophene, are selectively synthesized. Electrochemical and optical measurements of the parent NDTs indicated that the shape of the molecules plays an important role in determining the electronic structure of the compounds; the linear-shaped NDTs formally isoelectronic with naphthacene have lower oxidation potentials and more red-shifted absorption bands than those of the angular-shaped NDTs isoelectronic with chrysene. On the contrary, the performance of the thin-film-based field-effect transistors (FETs) using the dioctyl or diphenyl derivatives were much influenced by the symmetry of the molecules; centrosymmetric derivatives tend to give higher mobility (up to 1.5 $cm^2 V^{-1} s^{-1}$) than axisymmetric ones (~0.06 $cm^2 V^{-1} s^{-1}$), implying that the intermolecular orbital overlap in the solid state is influenced by the symmetry of the molecules. These results indicate that the present NDT cores, in particular the linear-shaped, centrosymmetric naphtho[2,3-*b*:6,7-*b*′]dithiophene, are promising building blocks for the development of organic semiconducting materials.

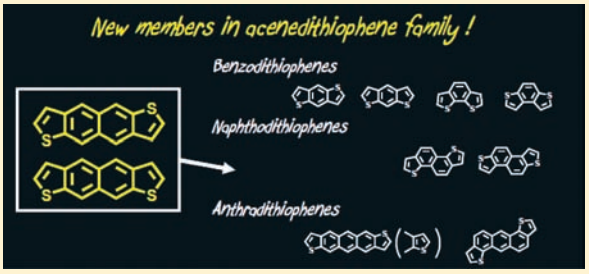

INTRODUCTION

Thiophene-fused polycyclic aromatic compounds (heteroarenes) have been attracting a great deal of interest in view of application to organic semiconducting materials for electronic device applications, such as organic field-effect transistors (OFETs)[1−4] and organic photovoltaics (OPVs).[5−7] In particular, linearly fused heteroarenes, benzodithiophene (BDT),[1] and anthradithiophene (ADT)[2] (Figure 1), an isoelectronic analogue of anthracene and pentacene, respectively, represent the usefulness of this class of compounds to, for example, solution- or vapor processable p- and n-channel organic semiconductors,[1−3] building block for polymers,[4] and synthetic intermediate for further extended heteroarenes.[8] In contrast to widely studied BDT and ADT derivatives whose efficient synthetic methods are well-documented,[9] linearly fused naphthodithiophenes (NDTs, **1** and **2**, Figure 1) isoelectronic with naphthacene have been yet to be synthesized, although the theoretical investigation predicts that they are promising cores for organic semiconductors.[10]

The isomeric NDTs with angular-fused structures (**3** and **4**, Figure 1) were recently isolated by Tobe et al. from a reaction mixture of the flash vacuum pyrolysis (FVP) of dithienyldienynes.[11a] On the other hand, we have devised a selective and scalable synthesis of **3** and applied the core to organic semiconducting materials.[12] In due course, the NDT framework of **3** was found to be useful not only as a core for molecular semiconductors[12] but also as a building unit for polymer semiconductors.[13] In fact, both the **3**-based molecular and polymer semiconductors are applicable to OFETs, and they showed field-effect mobility higher than 0.1 $cm^2 V^{-1} s^{-1}$. These fruitful results on **3** as well as the superiority of BDT and ADT as

Received: December 7, 2010
Published: March 09, 2011

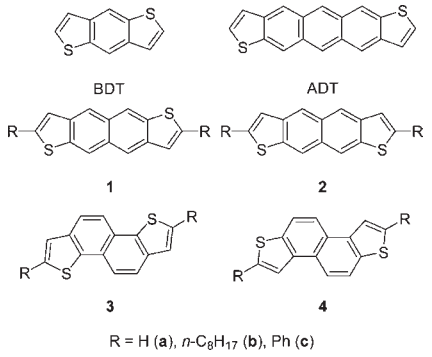

Figure 1. Molecular structures of BDT, ADT, and naphthodithiophene (NDT) isomers. **1**: naphtho[2,3-*b*:6,7-*b*′]dithiophenes, **2**: naphtho[2,3-*b*:7,6-*b*′]dithiophenes, **3**: naphtho[1,2-*b*:5,6-*b*′]dithiophenes, **4**: naphtho[2,1-*b*:6,5-*b*′]dithiophenes.

building blocks for electronic materials prompted us to study the linear-shaped NDTs, namely **1** and **2**.

In this paper, we first report a newly established selective syntheses of **1** and **2**. In the meantime, it turned out that the synthetic method developed for **1** and **2** is applicable to the selective synthesis of the angular-shaped NDT, **4**, which enables us to access all four NDT isomers (Figure 1), being promising cores for organic semiconductors, and thereby to compare their properties. We thus describe the comparison of electronic structures of the four parent NDTs (**1a**−**4a**) in detail. Then, the thin-film FET devices based on the dioctyl- (**1b**, **2b**, and **4b**) and diphenyl derivatives (**1c**, **2c**, and **4c**) are reported to evaluate the usefulness of the NDT cores for organic semiconductors. Among them, vapor-processed **1c**-based devices showed good FET characteristics with mobilities as high as 1.5 $cm^2 V^{-1} s^{-1}$ and I_{on}/I_{off} of 10^7, which is almost comparable with the isomeric 2,7-diphenyl[1]benzothieno[3,2-*b*][1]benzothiophene (DPh-BTBT)-based OFETs (~2.0 $cm^2 V^{-1} s^{-1}$).[3d] Finally, to get insight into the structure-properties relationship of the isomeric heteroarenes, detailed comparison between **1c** and DPh-BTBT were carried out in terms of the intermolecular orbital couplings in the solid state, molecular reorganization energy, and ionization potentials of the evaporated thin films.

RESULTS AND DISCUSSION

Synthesis. The reported selective synthesis of **3** is depicted in Scheme 1,[12] in which the thiophene annulation reaction from the precursor (**8**) with two *o*-chloroethynylbenzene substructures[9c] was employed as the key step for the synthesis. For the selective preparation of **8**, the higher reactivity of the trifluoromethanesulfonyloxy site than that of the chloro site in the Sonogashira coupling is crucial, and thus, 1,5-dichloro-2,6-bis(trifluoromethanesulfonyloxy)naphthalene (**7**), readily converted from 2,6-dihydroxynaphthalene (**6**), is the actual key intermediate for the synthesis of **3**.

For the synthesis of **1** and **2**, however, it is practically impossible to synthesize the counterparts of **7** possessing two chloro and trifluoromethanesulfonyloxy groups at the appropriate positions on the naphthalene core. Instead of the chloro intermediate, the bromo compounds (**10** and **13**, Scheme 2) were accessible via 3,7-dibromo-2,6-dihydroxynaphthalene (**9**) and 3,6-dibromo-2,7-dihydroxynaphthalene (**12**), respectively, via selective debromination reaction mediated by tin metal from

Scheme 1. Reported Synthesis of 3

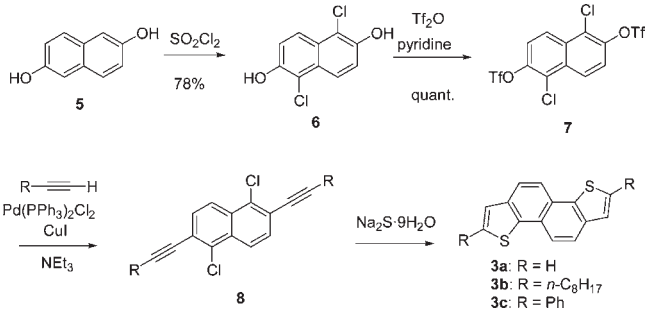

1,3,5,7-tetrabromo-2,6-dihydroxynaphthalene[14] and 1,3,6-tribromo-2,7-dihydroxynaphthalene,[15] respectively (Scheme 2). Being different from **7** with the chloro groups, the chemoselective Sonogashira coupling reactions of **10** and **13** at the trifluoromethanesulfonyloxy sites over the bromine sites seemed to be very difficult. After many attempted reactions under various conditions, however, we finally found that the reactions in polar solvents such as THF or DMF gave the desired products, **11** and **14**, with good selectivity in most cases (Scheme 2). The final ring closing reaction proceeded smoothly to give the parent, di-*n*-octyl, and diphenyl derivatives (**1a**−**c** and **2a**−**c**) in good yields.

The chemoselective Sonogashira coupling at the trifluoromethanesulfonyloxy sites over the bromine sites on the naphthalene derivatives also allowed synthesizing **4** from 1,5-dihydroxynaphthalene. It has been reported that bromination of 1,5-dihydroxynaphthalene gives 2,6-dibromo-1,5-dihydroxynaphthalene (**15**) selectively,[16] whereas chlorination takes places exclusively at 4- and 8-positions.[17] Thus, **15** was converted into the precursors (**17**) having the *o*-ethynylbromobenzene substructures via the trifluoromethanesulfonyloxy intermediate (**16**), and the final ring closing reaction with sodium sulfide gave **4a**−**c** in good yields. All the NDT derivatives (**1**, **2**, and **4**) were fully characterized with the spectroscopic and combustion elemental analyses (see Experimental section).

Physicochemical Properties. Cyclic voltammograms of the parent compounds, **1a**−**4a**, are shown in Figure 2a and their oxidation potentials are summarized in Table 1. Both **1a** and **2a** show quasi-reversible oxidation peaks at +0.94 V (onset, vs Ag/AgCl), indicating that **1a** and **2a** have almost the same HOMO energy levels. The good reversibility of their voltammograms implies that their oxidized species are electrochemically stable, and in fact, they did not polymerized on the working electrode even on repeated cycles (Figure S1, Supporting Information). These electrochemical behaviors of **1a** and **2a** sharply contrast to that of isomeric **3a**, which shows an irreversible oxidation peak at much higher oxidation potential (+1.38 V vs Ag/AgCl) and an electrochemical polymerization on the working electrode on the repeated cycles.[9] On the other hand, **4a** shows a rather similar electrochemical behavior to that of **3a**: relatively high oxidation potential (+1.33 V vs Ag/AgCl) to those of **1a** and **2a** and electrochemical polymerization on the electrode (Figure S1, Supporting Information). These results clearly indicate that the *direction* of thiophene rings fused on the naphthalene core (i.e., *anti* vs *syn* at the 2,3/6,7-fused position or 1,2-*b* vs 2,1-*b* annulation at the 1,2/5,6-fused position) does not affect to the electronic structures significantly, whereas the *position* of thiophene rings (i.e., 1,2/5,6-fused vs 2,3/6,7-fused) does (Table 1).

dx.doi.org/10.1021/ja110973m |*J. Am. Chem. Soc.* 2011, 133, 5024–5035

Scheme 2. Synthesis of 1, 2, and 4[a]

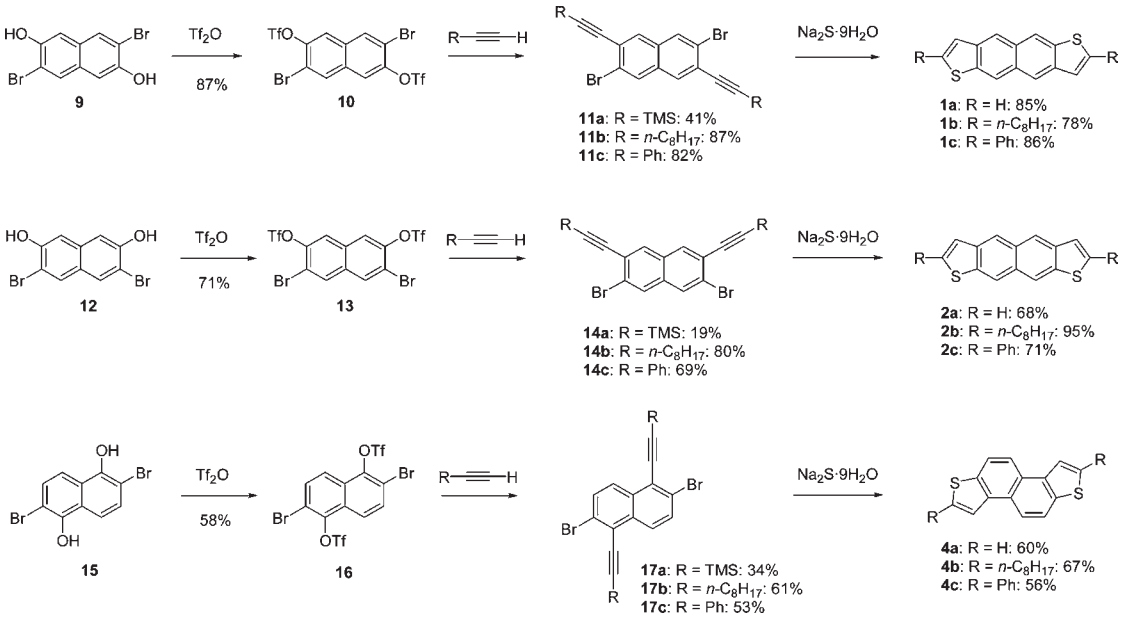

[a] TMS groups on the precursors (**11a**, **14a**, and **17a**) were removed spontaneously during the final ring closing reaction to give the parent NDTs.

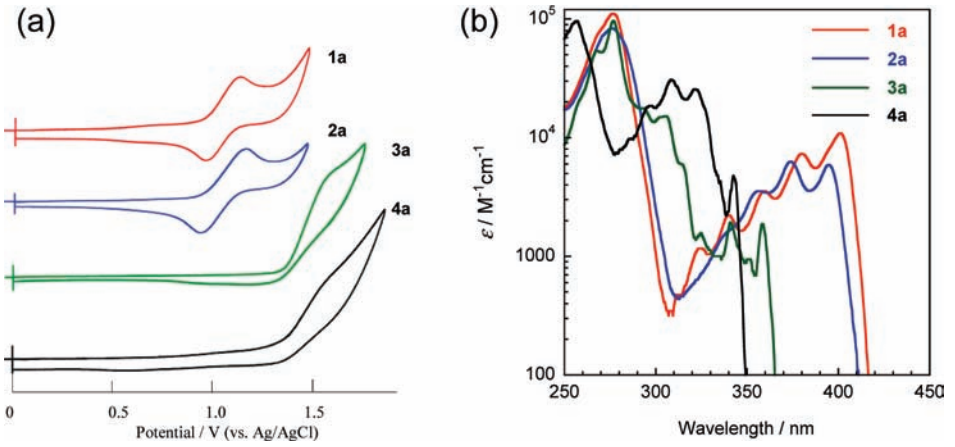

Figure 2. (a) Cyclic voltammograms and (b) UV−vis spectra of **1a**, **2a**, **3a**, and **4a**.

The difference in electronic structures can be qualitatively understood by considering the isoelectronic hydrocarbon-based fused aromatic systems. Apparently, **1a** and **2a** are isoelectronic with naphthacene with four benzene rings fused in a linear manner, whereas **3a** and **4a** are with chrysene with a kinked molecular structure.[18] The HOMO energy levels of acenes such as anthracene and naphthacene elevate significantly with increasing the number of the fused rings. However, the elevation of the HOMO energy level of the phenes such as phenanthrene and chrysene is not significant with increasing the number of the rings.[18,19] It is thus rational to consider that **3a** and **4a** isoelectronic with chrysene have higher oxidation potentials than those of **1a** and **2a**. These qualitative considerations are well reproduced by the theoretical calculations using the DFT methods,[20] which clearly show the similarity/difference of the energy levels of the frontier orbitals as well as the molecular electronic structures among **1a**−**4a** (Figure 3).

Absorption spectra of **1a** and **2a** in the solution are also similar to each other (Figure 2b), reflecting that these two isomers have basically the same electronic structures. Because of their acene-like structures, their absorption edges reach up to 410 nm, which is strikingly different from those of **3** and **4** (absorption edge: ∼350 nm) with the phene-like electronic structures.

It is already reported that photochemical- and oxidative-stability of large oligoacenes, such as naphthacene and pentacene are not very good.[21] In fact, absorption spectra of naphthacene in air-saturated solution under illumination of ambient light showed rapid degradation in several hours (Figure S2, Supporting Information). On the contrary, the absorption spectra of **1a** and **2a** under the identical conditions showed no apparent change even after several days, indicating that **1a** and **2a** are quite stable compounds, despite the fact that they are isoelectronic with naphthacene. These results show that the linear-fused heteroarenes (**1** and **2**) are promising building blocks with

dx.doi.org/10.1021/ja110973m |*J. Am. Chem. Soc.* 2011, 133, 5024–5035

Table 1. Electronic Properties of the Parent NDTs (1a−4a)

compound	E_{onset}/V[a]	HOMO/eV[b]	λ_{edge}/nm	E_g/eV[d]
1a	+0.94	−5.3	405	3.0
2a	+0.94	−5.3	410	3.1
3a	+1.38	−5.8	320[c]	3.9
4a	+1.33	−5.7	350	3.5
Naphthacene	+0.85	−5.2	490	2.5
Chrysene	+1.46	−5.9	330	3.8

[a] V vs Ag/AgCl. All the potentials were calibrated with the Fc/Fc^+ ($E^{1/2}$ = +0.43 V measured under identical conditions). [b] Estimated with a following equation: E^{HOMO} (eV) = −4.4 − E_{onset}. [c] Forbidden triplet−triplet bands were not considered (see ref 12). [d] Calculated from λ_{edge}.

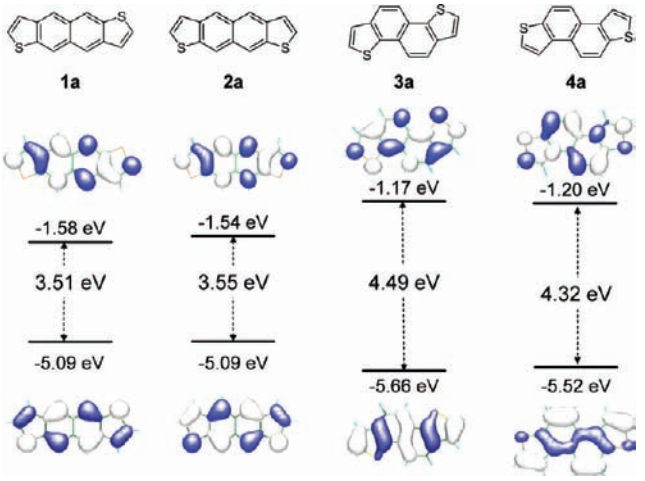

Figure 3. Calculated HOMOs and LUMOs of **1a**−**4a** with the TD-DFT B3LYP/6-31(d) level. The calculated electronic transition energies are 3.17 (**1a**), 3.20 (**2a**), 3.82 (**3a**), and 3.90 eV (**4a**).

relatively low oxidation potentials and good stability for the development of new organic semiconductors.[22]

Thin Film FET Devices of Dioctyl (1b−4b) and Diphenyl Derivatives (1c−4c). To evaluate the utility of **1**, **2**, and **4** as the core structure for organic semiconductors, we fabricated FET devices using vapor deposited thin films of the dioctyl- (**1b**, **2b**, and **4b**) and diphenyl derivatives (**1c**, **2c**, and **4c**) with a bottom gate, top-contact configuration on Si/SiO_2 substrates. Depicted in Figure 4 are the output- and transfer- characteristics of the FETs, and their field-effect mobilities (μ_{FET}) extracted from the saturation regime are summarized in Table 2.

As expected from the previous results on the related hetero-arene-based OFET devices,[3] both the dioctyl and diphenyl derivatives showed typical p-channel FET responses. Moreover, their FET characteristics were found to be largely dependent on the core structures and substituents. In case of the dioctyl derivatives, **1b** and **4b** with the centrosymmetic (C_{2h}) cores showed moderately high mobility (~0.3 $cm^2\ V^{-1}\ s^{-1}$), whereas **2b** with the axisymmetric (C_{2v}) core showed lower mobility (~0.015 $cm^2\ V^{-1}\ s^{-1}$) than those of **1b** and **4b** by 1 order of magnitude. Although the electronic structures of the NDT cores are determined by the molecular shapes, that is, the linear-shaped **1a** and **2a** are very similar to each other, but quite different from that of the angular-shaped **4a**, the transport properties in the FET devices are not the case. Rather than the molecular shape, the symmetry of the molecule seems to be an important factor that affects to the field-effect mobility in the thin film transistors.

Similar dependence of the mobilities on the symmetry of the core structure is observed for the diphenyl derivatives. The mobility of **1c**-based devices is among the highest (1.5 $cm^2\ V^{-1}\ s^{-1}$) with a large I_{on}/I_{off} ratio of 10^7, whereas **2c**-based ones showed lowest mobility (0.06 $cm^2\ V^{-1}\ s^{-1}$) among the present diphneyl NDT derivatives including previously reported **3c**-based ones (0.3 $cm^2\ V^{-1}\ s^{-1}$).[12]

Even though the semiconducting molecules are isoelectronic, the obvious differences between **1b**/**c**- and **2b**/**c**-based devices are quite striking and should be related to the difference of the symmetry, which may affect the intermolecular orbital overlap in the solid state (vide infra). On the other hand, **4c**-based FETs showed high mobility (0.80 $cm^2\ V^{-1}\ s^{-1}$), which is ca. three times higher than that of the isoelectronic **3c**-based one.[12] Although the reasons for the difference between the FET performances of **3c**- and **4c**-based devices are not very clear, we expect that the extent of the intermolecular orbital overlap through sulfur-involving nonbonded contacts in the solid state can be related; since the NDT core of **4** has two sulfur atoms in the molecular peripherally that face outwardly, whereas the sulfur atoms in the core of **3** reside in the bay region of the molecule, the former should be more favorable to the effective intermolecular interaction than the latter through no-bonded contacts involving sulfur atoms (vide infra).

Another point that should be addressed here is that, although the FET devices based on the centrocymmetric diphenyl derivatives (**1c** and **4c**) showed good performances comparable with that of the BTBT counterpart (DPh-BTBT, $\mu \approx 2.0$ $cm^2\ V^{-1}\ s^{-1}$),[3d] the FET mobilities of the octyl derivatives (**1b** and **4b**) -based devices are fairly low relative to those based on C_8−BTBT ($\mu \approx 2.9$ $cm^2\ V^{-1}\ s^{-1}$).[3k] To clarify these different tendencies depending on the substituent on the NDT cores, we then carried out structural investigations by means of XRD measurements on the evaporated thin films.

Thin Films of Dioctyl (1b−4b) and Diphenyl Derivatives (1c−4c). AFM images of evaporated thin films (Figure 5a−f) show distinct surface morphology depending on the substituents on the NDT cores. The thin films of the octyl derivatives (**1b**−**4b**) have a rather flat surface without clear grain boundary, whereas the surface of the thin films of diphenyl derivatives (**1c**−**4c**) consists of granulose crystallites. The size of the grains depends on T_{sub} for all the case (**1c**−**4c**) as observed for many related organic semiconductors; for **1c** and **2c**, the grain are ~0.1 μm in size for the thin films deposited at room temperature (section 8, Supporting Information), whereas ~0.2 μm at T_{sub} = 100 °C (Figure 5d and e). Apparently, the larger grains contribute to enhance μ_{FET} both for **1c** and **2c** (Table 2). On the other hand, when **4c** was deposited at high T_{sub}s, larger but noncontinuous crystallites were observed (section 8, Supporting Information), which is consistent with no field-effect response in actual devices.

Out-of-plane XRD patterns of the evaporated thin films (Figure 6a−f) show that these materials afford crystalline thin films with the lamella-like layered structure on the Si/SiO_2 substrate. The calculated interlayer spacing (*d*-spacing), molecular length obtained from the optimized molecular structure computed with the MOPAC-PM3 calculations, and the estimated molecular inclination from the substrate normal of **1b**−**4b** and **1c**−**4c** are listed in Table 3, together with their isomeric BTBT counterparts, C_8−BTBT and DPh-BTBT.

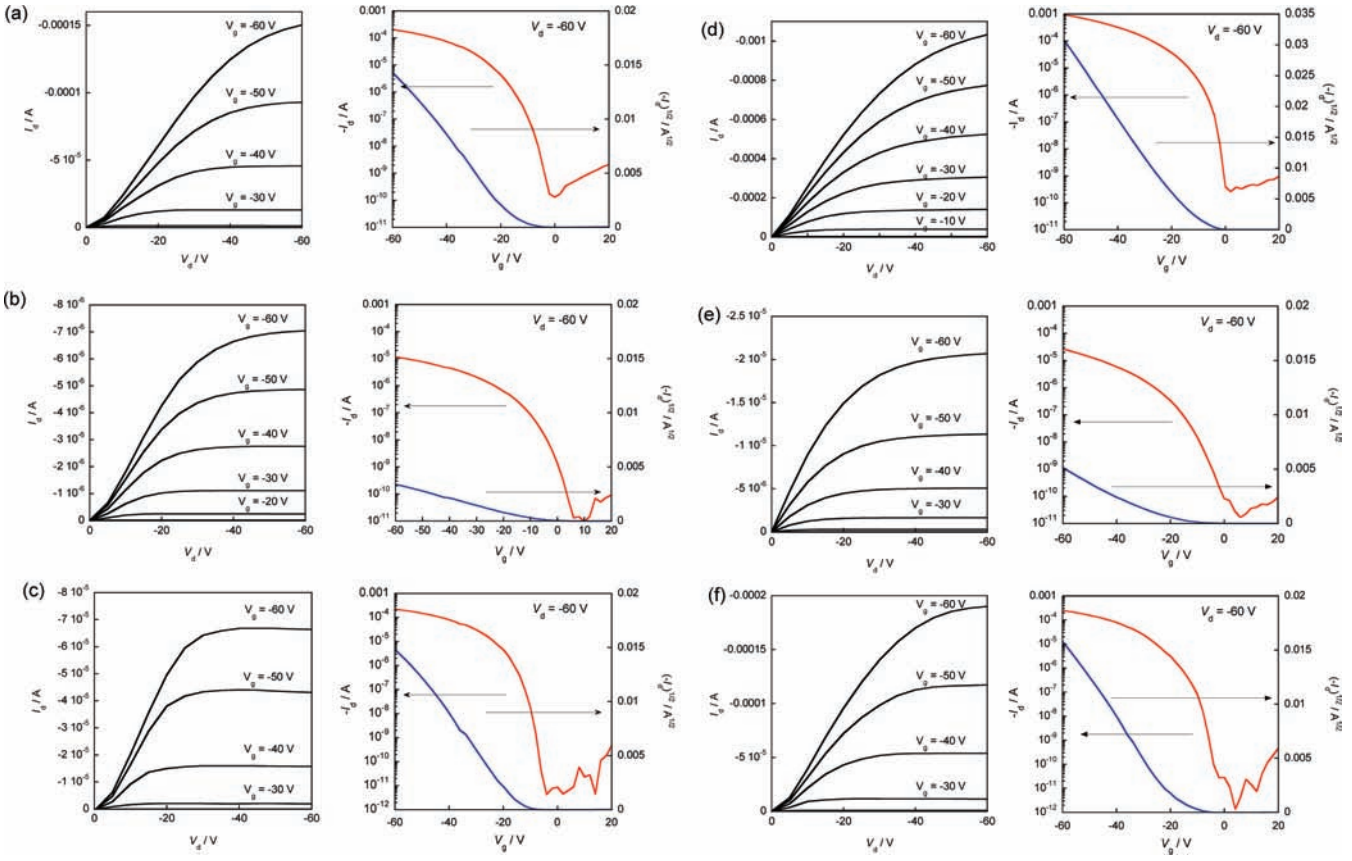

Figure 4. Output and Transfer characteristics of FETs fabricated on OTS-treated Si/SiO_2 substrate (T_{sub} = rt unless otherwise mentioned): (a) **1b**, (b) **2b**, (c) **4b**, (d) **1c** (T_{sub} = 100 °C), (e) **2c** (T_{sub} = 100 °C), and (f) **4c**.

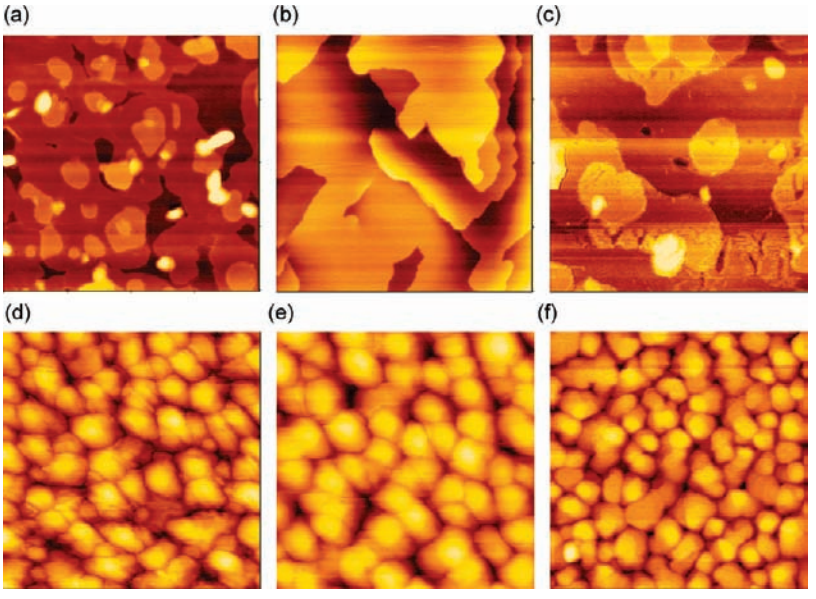

Figure 5. AFM images (2 × 2 μm) of evaporated thin films deposited on OTS-treated Si/SiO_2 substrate: (a) **1b**, (b) **2b**, (c) **4b**, (d) **1c** (T_{sub} = 100 °C), (e) **2c** (T_{sub} = 100 °C), and (f) **4c**.

The dioctyl derivatives of NDTs (**1b**, **2b**, **4b**) tend to show larger inclination (35−40°) than that of C_8−BTBT (30°), which is consistent with the observed lower mobilities of the formers (~0.3 $cm^2 V^{-1} s^{-1}$) than that of the latter (~2.9 $cm^2 V^{-1} s^{-1}$).[23] On the other hand, despite the fact that the mobilities of the vapor-processed devices are quite different between **1b** and **2b** by 1 order of magnitude, very similar thin film structures as well as molecular orientations are proposed for these isoelectronic NDT

dx.doi.org/10.1021/ja110973m |*J. Am. Chem. Soc.* 2011, 133, 5024–5035

derivatives by their XRD patterns. Theses contradictory results can be interpreted by the distinct intermolecular interaction caused by their different symmetry. In **1b** and **2b**, the relative positions of sulfur atoms with a large atomic radius, which influence the continuous intermolecular orbital overlap enhanced by sulfur-induced intermolecular contacts, are different; the centrosymmetric **1b** can afford delocalized intermolecular interaction over a wide range of molecular array through such intermolecular interactions, whereas axisymmetric **2b** containing the sulfur atoms at the same side of the molecular periphery tends to afford much localized intermolecular interaction between neighboring two molecules. This speculation is supported by their absorption spectra in the thin film state (Figure 7a); the centrosymmetric **1b** thin film shows a much-pronounced red shift than that for the **2b** thin film.

Different from the octyl derivatives, the molecules of the diphenyl derivatives tend to stand upright in the thin film state regardless of the central heteroarene core. Among these, very similar molecular ordering structure with almost the same interlayer distances (d = ca. 20 Å) are suggested for the **1c** and **2c** thin films as in the case for previously discussed **1b** and **2b**. Considering the large difference of the FET mobilities between these two, it is speculated that the difference in the intermolecular interaction caused by the molecular symmetry again plays crucial role for the transport properties in the thin film state. In this case also, a distinct red-shifted absorption was observed for the **1c** thin film (Figure 7b), indicating the different extents of the intermolecular interaction for **1c** and **2c** in the thin film state.

Table 2. FET Characteristics[a] of 1b-, 2b-, 4b-, 1c-, 2c-, 3c-, and 4c-Based OFETs Fabricated on OTS-Treated Si/SiO_2 Substrate

compound	T_{sub}[b]/°C	μ_{FET}[c] $cm^2\ V^{-1}\ s^{-1}$	I_{on}/I_{off}[d]	V_{th}/V
1b[e]	rt	0.20	10^6	−19
2b[e]	rt	0.015	10^6	−21
4b[e,f]	rt	0.30	10^5	−10
1c	rt	0.50	10^5	−5
	60	0.80	10^7	−5
	100	1.5	10^7	−5
2c	rt	0.030	10^6	−16
	60	0.050	10^6	−21
	100	0.060	10^7	−22
3c[f,g]	100	0.30	10^5	−32
4c[e]	rt	0.80	10^6∼10^7	−20

[a] FET devices were fabricated on octyltrichlorosilane (OTS)-treated substrates with W/L = 30 unless otherwise stated. [b] Substrate temperature during vapor deposition of the semiconductors. The mobility values are typical ones from more than ten devices tested. [c] extracted from the saturation regime. [d] I_{on} and I_{off} were the source-drain current measured at V_g = −60 V and V_g = 0 V, respectively. [e] Vapor deposition at high T_{sub} gave no continuous thin films. [f] Data from the devices fabricated on hexamethyldisilazane (HMDS)-treated Si/SiO_2 substrate. [g] See ref 12.

Single Crystal X-Ray Structural Analysis of 1c and 4c. Single crystals of **1c** and **4c** with sufficient quality for X-ray structural analysis were grown in careful recrystallization, although single crystals of other compounds suitable for the analysis were not obtained. Their packing structures are depicted in Figures 7 and 8, respectively.

The simulated powder pattern from the bulk **1c** crystal (Figure S3, Supporting Information) well reproduces the XRD pattern of the evaporated thin film of **1c** (Figure 6d), suggesting that the both phases are the same. The packing structure of **1c** well represents the typical organic semiconductor's one, where the planar **1c** molecules pack efficiently in the layer-by-layer structure with the molecular long axis direction along the crystallographic c-axis (Figure 8a). The **1c** layer in the crystallographic ab plane consists of a herringbone packing structure reminiscent of high performance organic semiconductors such as pentacene (Figure 8b). No strong intermolecular sulfur−sulfur contacts shorter than the sum of van der Waals radii (∼3.6 Å) is observed

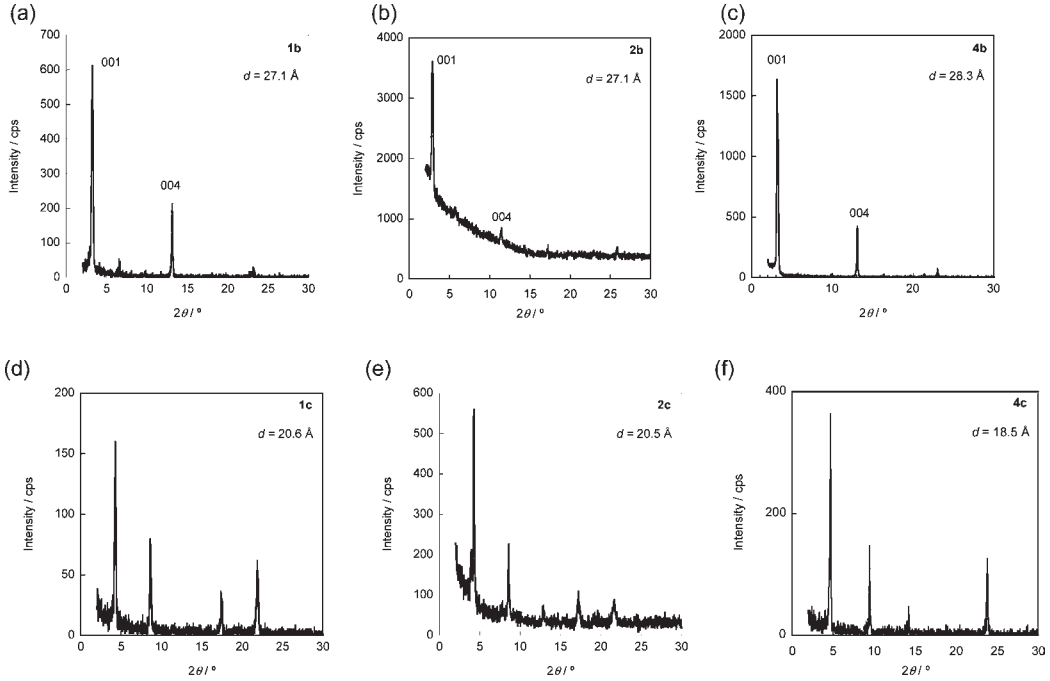

Figure 6. Out-of-plane XRDs of the evaporated thin films deposited on OTS-treated Si/SiO_2 substrate: (a) **1b**, (b) **2b**, (c) **4b**, (d) **1c**, (e) **2c**, and (f) **4c**.

dx.doi.org/10.1021/ja110973m |*J. Am. Chem. Soc.* 2011, 133, 5024–5035

Table 3. Interlayer Spacings (*d*-Spacings) of Evaporated Thin Films on the Si/SiO_2 Substrate of 1b, 2b, 4b, 1c, 2c, and 4c

compound	$2\theta/^{\circ}$ [a]	*d*-spacings[b]/Å	molecular length (*l*)/Å[c]	inclination (θ_{tilt}) from the substrate normal/° [d]
1b	3.26	27.1	30.8	40
2b	3.26	27.1	30.8	40
4b	3.12	28.3	30.7	35
1c	4.28	20.6	20.2 (19.97)	0
2c	4.30	20.5	20.0	0
4c	4.76	18.5	19.0 (18.67)	0
C_8–BTBT[e]	3.05	28.9	30.8 (30.11)	30
DPh-BTBT[f]	4.54	19.4	19.7 (19.22)	0

[a] (001) peaks. [b] Calculated interlayer spacings from the (001) reflections. [c] Obtained from optimized molecular geometry using MOPAC-PM3-MO calculations. Values in parentheses are obtained from X-ray structural analyses. [d] Determined as $\theta_{tilt} = \cos^{-1}(d/l)$. [e] See also refs 3g and 3k. [f] See also ref 3d.

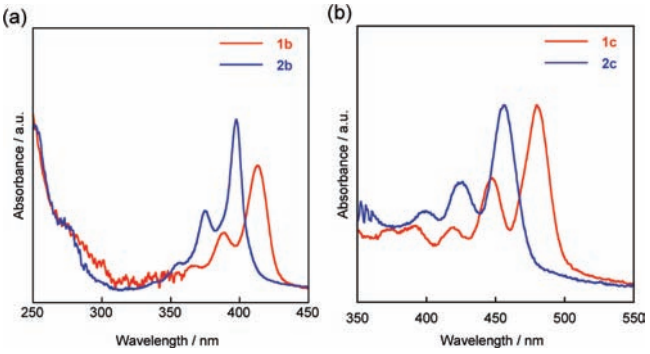

Figure 7. Absorption spectra of thin films of (a) **1b** and **2b** and (b) **1c** and **2c**.

in the **1c** layer, instead, there exists the molecular ribbon-like networks with sulfur–sulfur (~3.88 Å) and edge-to-face CH–π (~2.84 Å) contacts in the crystallographic (−1 1 0) and (1 1 0) directions. We thus conclude that the pronounced red shift of **1c** thin film (Figure 7b) as well as the better mobility of **1c**-based FET than that of **2c** should originate from the continuous intermolecular interaction based on the centrosymmetric (C_{2h}) structure of **1c**. Although the exact crystal structure of **2c** is not clear, the kind of intermolecular network structure could be very difficult to occur for **2c** with C_{2v} symmetry.

Different from **1c**, where the structures both in the thin film and the bulk single crystal are likely the same, the single crystal structure of **4c** in the bulk crystal is apparently different from that in the thin film, judged from the comparison of the XRD pattern of the thin film (Figure 6f) and the simulated powder pattern (Figure 9c). Thus, it is not appropriate to correlate directly between the crystal structure in the bulk single crystal phase and the transport properties in the thin film state. Nevertheless, careful inspection of the packing structure in the bulk single crystal of **4c** would be beneficial to understand its structural features in the solid state. In the actual crystal structure, the **4c** molecules form stacking structures along the crystallographic *b*-axis direction with an interplanar separation of ca. 3.3 Å (Figure 9a). In addition, the molecular stacks interact to one another via sulfur–sulfur contacts (3.71 Å) with the edge-to-face manner (Figure 9b). The latter interactive structure via sulfur atoms should be characteristic of **4c** with two sulfur atoms pointing outward, since the isoelectronic **3c** with the sulfur atoms in the molecular bay region did not show such interactive short S–S contacts (Figure S4, Supporting Information).[12] We thus speculate that such effective intermolecular interaction between **4c** molecules is also operative in the thin film phase and thus can rationalize the higher mobility of **4c**-based devices than that of **3c**.

Detailed Comparison of 1c and DPh-BTBT. Above discussions based on the XRD studies gave qualitative understanding of the structure–property relationships within the NDT-based organic semiconductors and the rationale for the fact that **1c** gave the best FET performances among the present NDT-based organic semiconductors. In fact, the mobility of **1c**-based FETs as high as 1.5 $cm^2\ V^{-1}\ s^{-1}$ is comparable to those of the recently developed superior organic semiconductors including DPh-BTBT. Interestingly, the core structures of BTBT and NDT are isomeric to each other with two thiophene and two benzene rings fused in linear manners. Thus, it is very interesting to compare these two isomeric high-performance organic semiconductors in detail, which will give us an insight into the electronic structures both at the solid state as well as the molecular levels.

First, to qualitatively understand the electronic structures in the solid state, we carried out calculations of transfer integrals (*t*) between HOMOs in the semiconducting layer elucidated by the single crystal X-ray analysis using the Amsterdam Density Functional (ADF) program package.[24,25] Calculated transfer integrals are shown in Figure 9. For **1c**, both the transfer integrals along the stacking direction designated as t_a (19 meV) and those in the side-by-side direction designated as t_p and t_q (61 and 58 meV, respectively) are quite large, indicating that the two-dimensional strong intermolecular orbital coupling is realized as observed for high performance organic semiconductors (Figure 10a).[26,27] Similarly, large transfer integrals both in the stacking (t_a: 34 meV) and transverse directions (t_p: 65 meV) are also calculated for DPh-BTBT (Figure 10b). These results are quite reasonable and consistent with their similar high mobilities. However, detailed comparison of these two implies that the difference of the core structure may cause the subtle change in the solid-state electronic structure. When compared the transfer integrals in the stacking (t_a) and the transverse directions (t_p and t_q), t_a in the **1c** structure is ca. one-third of t_p or t_q, indicating that moderate anisotropy for **1c** could be likely. In case of the DPh-BTBT structure, t_a:t_p ratio is 1:2, implying the smaller anisotropy for DPh-BTBT than that for **1c**. Note that the BTBT core structure has two sulfur atoms in the center of the molecule, facilitating direct sulfur–sulfur intermolecular contacts. In fact, nonbonded intermolecular sulfur–sulfur distance in DPh-BTBT crystal is 3.51 Å, which is much shorter than the sum of the van deer Waals radii of sulfur atom (3.60 Å), in the molecular stacks

dx.doi.org/10.1021/ja110973m |*J. Am. Chem. Soc.* 2011, 133, 5024–5035

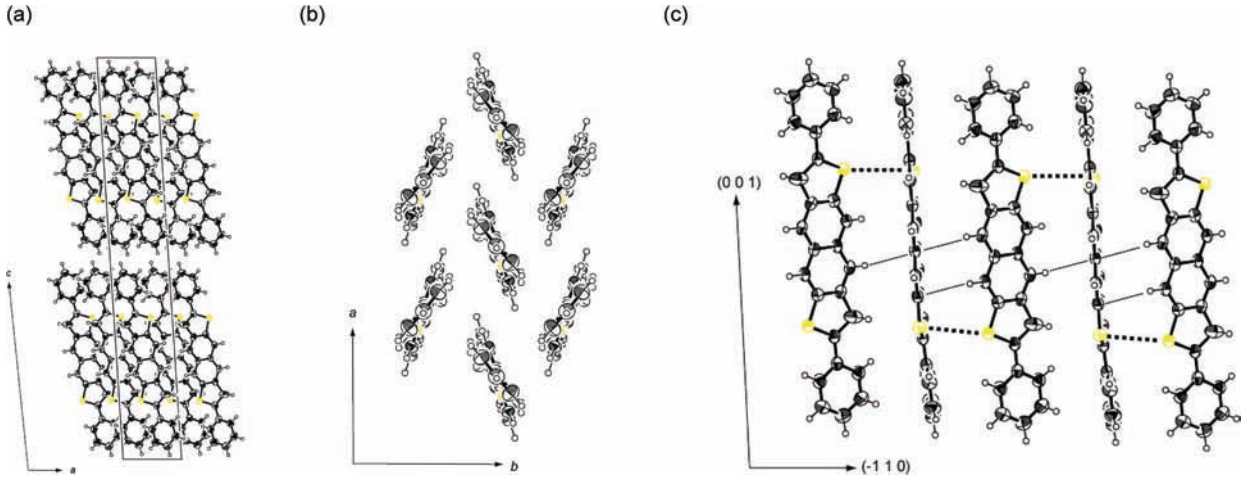

Figure 8. Packing structure of **1c** representing the typical molecular lamella structure (a) with a herringbone packing motif (b). Face-to-edge molecular array with nonbonded weak sulfur−sulfur contacts (dotted line: 3.86−3.88 Å) and edge-to-face CH-π contacts (solid line: 2.83−2.84 Å) also exist (c).

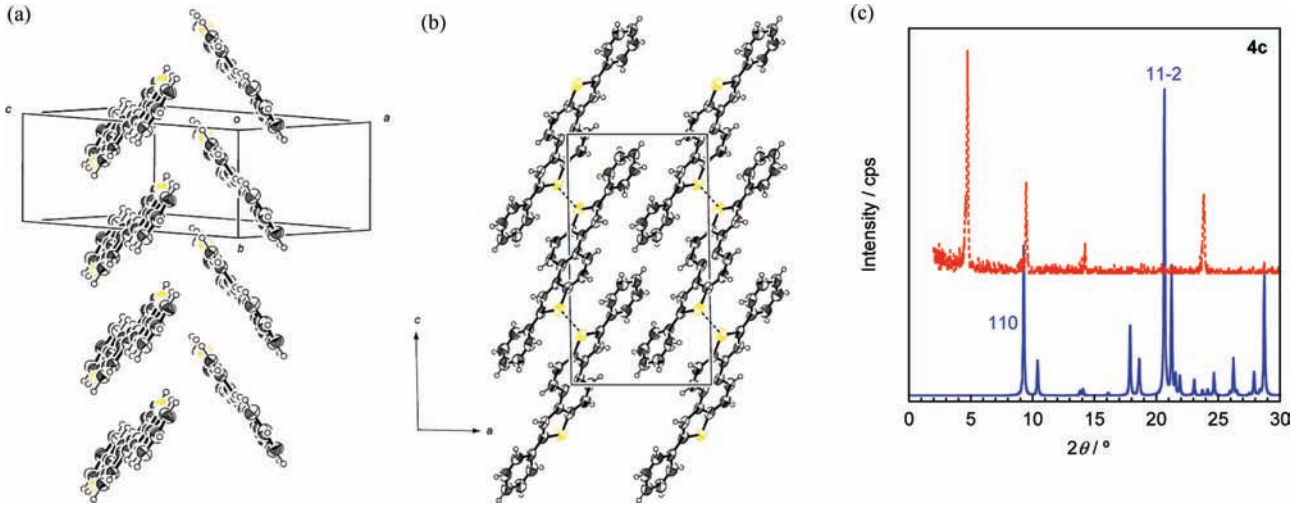

Figure 9. Packing structure of **4c**: (a) stacking structure along the *b*-axis direction, (b) *b*-axis projection (dotted line: 3.71 Å), and (c) simulated powder pattern from the bulk single crystal of **4c** (blue solid line), which is apparently different from that of the evaporated thin film (red dotted line, Figure 6f).

along the crystallographic *a*-axis direction, which certainly contributes to the larger t_a than that in the **1c**. In contrast, no such short sulfur−sulfur contact exists in the **1c** crystal structure, thereby resulting in small t_a. Thus, the large t_a and thereby small anisotropy in the solid-state electronic structure of DPh-BTBT can be boiled down to the molecular structure level.[28]

Another important parameter that may potentially affect the transport properties is molecular reorganization energy (λ).[29] In the present p-channel organic semiconductors' cases, λ for hole (λ^h) should be in concern, and λ^hs for the cores, that is, **1a** and the parent BTBT, are calculated to be 105 and 226 meV, respectively.[10,19] The smaller λ^h for **1a** than that of BTBT can be qualitatively understood by the consideration that the **1a** has an acene-like electronic structure that is an ideal structure for minimizing λ.[10,30] From the viewpoint of λ^h, the core structure of **1a** should be advantageous for efficient carrier transport. However, in case of the diphenyl derivatives, the difference in λ^h is much smaller than the parent (λ^h; **1c**: 170 meV, DPh-BTBT: 233 meV), implying that the effect from the difference of λ^h may be rather marginal.

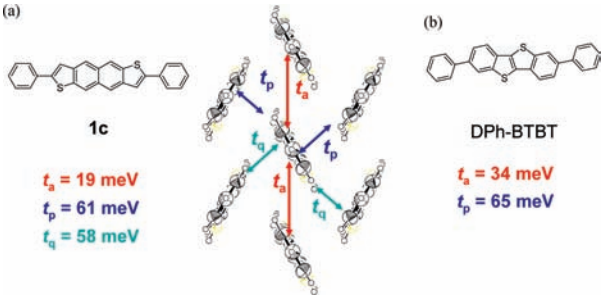

Figure 10. Calculated transfer integrals of the semiconducting layer of (a) **1c** and (b) DPh-BTBT.

Finally, we shall mention their molecular electronic structures that determine their HOMO energy levels. As already discussed, the NDT core (**1a**) is isoelectronic with naphthacene, whereas the BTBT core is with chrysene.[18] Since **1c** is hardly soluble to common organic solvents, it is not possible to estimate its

dx.doi.org/10.1021/ja110973m |*J. Am. Chem. Soc.* 2011, 133, 5024–5035

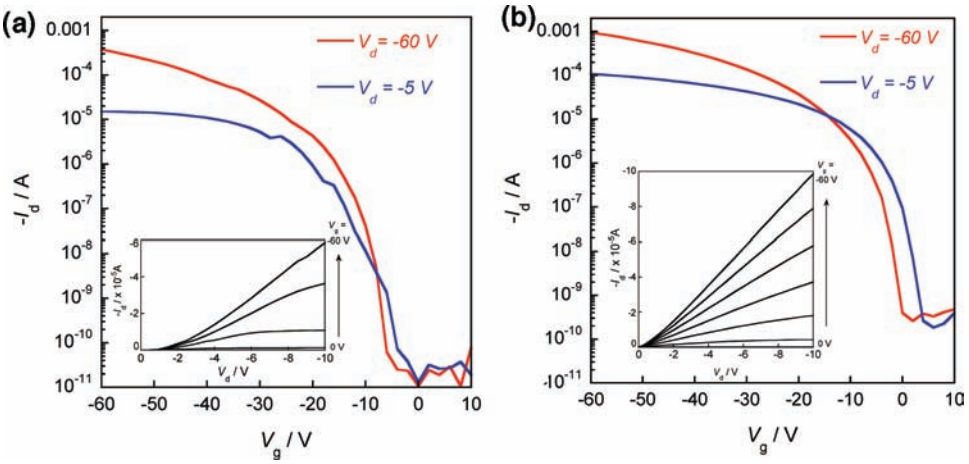

Figure 11. FET characteristics of (a) DPh-BTBT- and (b) **1c**-based devices in the linear (V_d = −5 V) and saturated regimes (V_d = −60 V) (insets: output characteristics at the low V_d region).

HOMO energy level with electrochemical methods. Instead, we measured the ionization potentials (IP) of the evaporated thin films of **1c** and DPh-BTBT with photoemission yield spectroscopy in air. The IP of DPh-BTBT (5.6 eV) is relatively high to ordinary organic semiconductors such as pentacene (5.0 eV).[3d] In contrast, the IP of **1c** is determined to be 5.1 eV, which is very close to that of pentacene. It has been pointed out that large IP (i.e., deep HOMO energy level) often causes large contact resistance between the gold source electrode (work function: ~5.0 eV) and the semiconducting layer that gives rise to poor FET characteristics in the linear regime,[31] although it brings enhanced air-stability.[32] In fact, the FET characteristics of DPh-BTBT-based devices in the linear regime (V_d = −5 V) are much influenced by the large contact resistance; the FET mobility in the linear regime (μ_{lin}: ~0.1 cm^2 V^{-1} s^{-1}) is less than one tenth of that in the saturated regime (μ_{sat}: ~1.5 cm^2 V^{-1} s^{-1}), and nonlinear behavior at the low V_d region was observed (Figure 11a). In contrast, such effects from the contact resistance are not siginificant for the **1c**-based devices (Figure 11b); μ_{lin}: 1.0 cm^2 V^{-1} s^{-1} and almost linear increase of I_d at the low V_d region. This can be ascribed to smaller IP of **1c** than that of DPh-BTBT. In addition to the small contact resistance, **1c**-based devices showed fairly good air stability; even after storage under ambient lab conditions during several months (Figure S5, Supporting Information), the devices showed basically no degradation at all. As a result, **1c** is a potential organic semiconductor that can give high mobility FETs with good air stability and low contact resistance.

CONCLUSION

In summary, we have successfully established selective and straightforward synthetic routes to linear-and angular-shaped NDTs (**1**, **2**, and **4**). Physicochemical evaluation of the parent NDTs revealed that linear-shaped **1a** and **2a** have lower oxidation potentials than those of angular-shaped **3a** and **4a**, reflecting that **1a** and **2a** are formally isoelectronic with naphthacene, whereas **3a** and **4a** are with chrysene. These results indicate that the *direction* of thiophene rings fused on the naphthalene core (i.e., *anti* vs *syn* at the 2,3/6,7-fused position or 1,2-*b* vs 2,1-*b* annulation at the 1,2/5,6-fused position) does not largely affect to the electronic structures, whereas the *position* of thiophene rings (i.e., 1,2/5,6-fused vs 2,3/6,7-fused) is crucial to determine the molecular electronic structure of the resulting heteroarenes.

In contrast to the molecular properties, the device characteristics are fairly influenced by the symmetry of the molecules, and centrosymmetric **1** and **4** gave high performance OFETs with mobilities higher than 0.1 cm^2 V^{-1} s^{-1}. Among the present NDT-based organic semiconductors, the diphenyl derivative of the linear-shaped, centrosymmetric one (**1c**) gave the best devices showing mobilities of up to 1.5 cm^2 V^{-1} s^{-1} with I_{on}/I_{off} of 10^7. The high mobility of **1c**-based transistor is well interpreted by the elucidation of the solid-state electronic structure based on the molecular arrangement. Not only the high mobility, its good performances were preserved for more than one month under ambient conditions, showing the air-stability of the OFET devices as well as the material itself. Moreover, facile carrier injection from the gold electrode into the semiconducting layer and thus fairly good FET characteristics in the linear regime were observed for the **1c**-based devices, reflecting the lower IP of the semiconductor (5.1 eV) than that of isomeric DPh-BTBT (5.6 eV) showing comparable FET mobility to that of **1c**. These are important experimental evidence that indicates the linear-shaped, centrosymmetric NDT (**1**) is a highly promising core structure for developing new organic semiconducting materials that simultaneously assume high stability and good carrier injection/transport properties. For these reasons, further material developments based on **1**, both for small molecules and polymeric materials, by making use of the chemically reactive α positions of the thiophene moieties, are now actively investigated in our group.

EXPERIMENTAL SECTION

Synthesis. *General.* All chemicals and solvents are of reagent grade unless otherwise indicated. THF was purified with a standard distillation procedure prior to use. 1,3,5,7-Tetrabromo-2,6-dihydroxynaphthalene,[14] 3,6-dibromo-2,7-dihydroxynaphthalene,[15] 2,6-dibromo-1,5-dihydroxynaphthalene[16] were synthesized as reported. Melting points were uncorrected. All reactions were carried out under nitrogen atmosphere. Nuclear magnetic resonance spectra were obtained in deuterated chloroform ($CDCl_3$) with TMS as internal reference unless otherwise stated; chemical shifts (δ) are reported in parts per million. IR spectra were recorded using a KBr pellet for solid samples. EI-MS spectra were obtained using an electron impact ionization procedure (70 eV).

3,7-Dibromo-2,6-dihydroxynaphthalene (9). To a suspension of 1,3,5,7-tetrabromo-2,6-dihydroxynaphthalene[14] (1.0 g, 2.1 mmol) in glacial acetic acid (20 mL) was added mossy tin (499 mg, 4.2 mmol) and the mixture was refluxed for 62 h. After cooling to room temperature, water (20 mL) was added to the mixture. The resulting precipitate was collected by filtration and washed with water to give 2,6-dibromo-3,7-dihydroxynaphthalene (**9**, 530 mg, 79%) as a white solid. Mp 243−245 °C; ^{1}H NMR (400 MHz, $CDCl_3$) δ 5.58 (s, 2H), 7.25 (s, 2H), 7.89 (s, 2H); ^{13}C NMR (100 MHz, DMSO-d_6) δ 109.1, 113.6, 128.8, 129.8, 149.9; EI-MS (70 eV) m/z = 316 (M^+); IR (KBr) ν = 3265 (OH) cm^{-1}; Anal. Calcd for $C_{10}H_6Br_2O_2$: C, 37.77; H, 1.90%. Found: C, 37.77; H, 1.77%.

General Procedure for the Triflation of Dibromodihydroxynaphthalene. To a suspension of dibromodihydroxynaphthalene (3.0 g, 9.4 mmol), pyridine (4.5 mL, 56 mmol) in dichloromethane (90 mL) was slowly added trifluoromethanesulfonic anhydride (3.3 mL, 21 mmol) at 0 °C. After the mixture was stirred for 4 h at room temperature, water (10 mL) and hydrochloric acid (1 M, 10 mL) were added. The resulting mixture was extracted with dichloromethane (30 mL × 3), and combined organic layer was dried ($MgSO_4$) and concentrated in vacuo. The residue was purified by column chromatography on silica gel eluted with dichloromethane (R_f = 0.95) to give dibromobis(trifluoromethanesulfonyloxy)naphthalene as a white solid.

3,7-Dibromo-2,6-bis(trifluoromethanesulfonyloxy)naphthalene (10). Seventy-one percent yield. Mp 138−139 °C; ^{1}H NMR (270 MHz, $CDCl_3$) δ 7.14 (s, 2H), 8.25 (s, 2H); ^{13}C NMR (68.5 MHz, $CDCl_3$) δ 116.2, 118.8 (q, $^2J_{C-F}$ = 318.8 Hz, CF_3), 120.0, 131.9, 133.9, 145.8; EI-MS (70 eV) m/z = 580 (M^+); Anal. Calcd for $C_{12}H_4Br_2F_6O_6S_2$: C, 24.76; H, 0.69%. Found: C, 24.80; H, 0.29%.

3,6-Dibromo-2,7-bis(trifluoromethanesulfonyloxy)naphthalene (13). Sixty percent yield. Mp 123−124 °C; ^{1}H NMR (400 MHz, $CDCl_3$) δ 7.86 (s, 2H), 8.19 (s, 2H); ^{13}C NMR (100 MHz, $CDCl_3$) δ 116.5, 118.8 (q, $^2J_{C-F}$ = 319.3 Hz, CF_3), 121.1, 131.3, 132.5, 132.8, 145.7; EI-MS (70 eV) m/z = 580 (M^+); Anal. Calcd for $C_{12}H_4Br_2F_6O_6S_2$: C, 24.76; H, 0.69%. Found: C, 25.03; H, 0.39%.

2,6-Dibromo-1,5-bis(trifluoromethanesulfonyloxy)naphthalene (15). Fifty-eight percent yield. Mp 159−160 °C; ^{1}H NMR (270 MHz, $CDCl_3$) δ 7.89 (d, J = 9.2 Hz 2H), 8.03 (d, J = 9.2 Hz 2H); ^{13}C NMR (100 MHz, $CDCl_3$) δ 116.8, 118.8 (q, $^2J_{C-F}$ = 319.4 Hz, CF_3), 123.0, 128.8, 133.3, 142.7; EI-MS (70 eV) m/z = 580 (M^+); Anal. Calcd for $C_{12}H_4Br_2F_6O_6S_2$: C, 24.76; H, 0.69%. Found: C, 25.03; H, 0.35%.

General Procedure for the Palladium-Catalyzed Sonogashira Coupling of Dibromobis(trifluoromethanesulfonyloxy)naphthalene with Terminal Alkynes. To a degassed solution of dibromobis(trifluoromethanesulfonyloxy)naphthalene (582 mg, 1.0 mmol) in DMF (7 mL) and diisopropylamine (7 mL) was added $Pd(PPh_3)_2Cl_2$ (70 mg, 0.05 mmol, 10 mol %), CuI (38 mg, 0.1 mmol, 20 mol %) and terminal alkyne (2.0 mmol). After the mixture was stirred for 11 h at room temperature, water (1 mL) and hydrochloric acid (1 M, 1 mL) were added. The resulting mixture was extracted with dichloromethane (5 mL × 3), and the combined organic layer was dried ($MgSO_4$) and concentrated in vacuo. The residue was purified by column chromatography on silica gel eluted with hexane to give dibromodiethynylnaphthalene analogue as a white solid.

2,6-Dibromo-3,7-bis(trimethylsilylethynyl)naphthalene (11a). Forty-one percent yield. Mp 196−197 °C; ^{1}H NMR (270 MHz, $CDCl_3$) δ 0.30 (s, 18H), 7.87 (s, 2H), 7.97 (s, 2H); ^{13}C NMR (100 MHz, $CDCl_3$) δ −0.1, 101.4, 102.8, 123.2, 124.5, 130.6, 131.9, 132.2; EI-MS (70 eV) m/z = 478 (M^+); Anal. Calcd for $C_{20}H_{22}Br_2Si_2$: C,50.22; H, 4.64%. Found: C, 50.43; H, 4.65%.

2,6-Dibromo-3,7-di(decyn-1-yl)naphthalene (11b). Eighty-seven percent yield. Mp 98−99 °C; ^{1}H NMR (270 MHz, $CDCl_3$) δ 0.89 (t, J = 7.0 Hz, 6H), 1.27−1.37 (m, 20H), 1.61−1.72 (m, 4H), 2.51 (t, J = 6.6 Hz, 4H) 7.79 (s, 2H), 7.95 (s, 2H); ^{13}C NMR (100 MHz, $CDCl_3$) δ 14.3, 19.8, 22.8, 28.7, 29.1, 29.3, 29.4, 32.0, 79.4, 96.9, 123.4, 124.8, 130.3, 131.4, 131.6; EI-MS (70 eV) m/z = 558 (M^+); Anal. Calcd for $C_{30}H_{38}Br_2$: C,64.52; H, 6.86%. Found: C, 64.59; H, 6.87%.

2,6-Dibromo-3,7-bis(phenylethynyl)naphthalene (11c). Eighty-two percent yield. Mp 213−214 °C; ^{1}H NMR (400 MHz, $CDCl_3$) δ 7.39−7.41 (m, 6H), 7.62−7.64 (m, 4H) 7.97 (s, 2H), 8.07 (s, 2H); ^{13}C NMR (100 MHz, $CDCl_3$) δ 88.1, 95.3, 122.8, 123.4, 124.6, 128.6, 129.1, 130.7, 131.6, 132.0; EI-MS (70 eV) m/z = 486 (M^+); Anal. Calcd for $C_{26}H_{14}Br_2$: C,64.23; H, 2.90%. Found: C, 64.11; H, 2.60%.

3,6-Dibromo-2,7-bis(trimethylsilylethynyl)naphthalene (14a). Nineteen percent yield. Mp 168−170 °C; ^{1}H NMR (270 MHz, $CDCl_3$) δ 0.30 (s, 18H), 7.90 (s, 2H), 7.95 (s, 2H); ^{13}C NMR (100 MHz, $CDCl_3$) δ −0.1, 100.9, 102.8, 123.8, 124.2, 130.0, 130.0, 133.0, 133.6; EI-MS (70 eV) m/z = 478 (M^+); Anal. Calcd for $C_{20}H_{22}Br_2Si_2$: C,50.22; H, 4.64%. Found: C, 49.93; H, 4.45%.

3,6-Dibromo-2,7-di(decyn-1-yl)naphthalene (14b). Eighty percent yield. Mp 50−51 °C; ^{1}H NMR (270 MHz, $CDCl_3$) δ 0.89 (t, J = 6.8 Hz, 6H), 1.27−1.72 (m, 24H), 2.50 (t, J = 6.9 Hz, 4H) 7.81 (s, 2H), 7.93 (s, 2H); ^{13}C NMR (100 MHz, $CDCl_3$) δ 14.3, 19.8, 22.8, 28.7, 29.1, 29.3, 29.4, 32.0, 79.4, 96.5, 124.0, 124.5, 129.7, 130.3, 132.0, 132.8; EI-MS (70 eV) m/z = 558 (M^+); Anal. Calcd for $C_{30}H_{38}Br_2$: C,64.52; H, 6.86%. Found: C, 64.49; H, 6.74%.

3,6-Dibromo-2,7-bis(phenyletynyl)naphthalene (14c). Sixty-nine percent yield. Mp 164−165 °C; ^{1}H NMR (270 MHz, $CDCl_3$) δ 7.38−7.42 (m, 6H), 7.62−7.65 (m, 4H), 8.01 (s, 2H), 8.03 (s, 2H); ^{13}C NMR (100 MHz, $CDCl_3$) δ 88.0, 94.8, 122.8, 124.0, 124.2, 128.6, 129.0, 130.1, 130.3, 131.9, 132.4, 133.5; EI-MS (70 eV) m/z = 486 (M^+); Anal. Calcd for $C_{26}H_{14}Br_2$: C,64.23; H, 2.90%. Found: C, 64.33; H, 2.67%.

2,6-Dibromo-1,5-bis(trimethylsilylethynyl)naphthalene (17a). Thirty-four percent yield. Mp 201−202 °C; ^{1}H NMR (270 MHz, $CDCl_3$) δ 0.35 (s, 18H), 7.71 (d, 2H, J = 8.8 Hz), 8.14 (d, 2H, J = 8.8 Hz); ^{13}C NMR (100 MHz, $CDCl_3$) δ 0.1, 100.8, 106.6, 123.0, 126.0, 128.1, 131.5, 133.1 EI-MS (70 eV) m/z = 478 (M^+); Anal. Calcd for $C_{20}H_{22}Br_2Si_2$: C,50.22; H, 4.64%. Found: C, 49.98; H, 4.49%.

2,6-Dibromo-1,5-di(decyn-1-yl)naphthalene (17b). Sixty-one percent yield. Mp 70−71 °C; ^{1}H NMR (270 MHz, $CDCl_3$) δ 0.89 (t, 6H, J = 6.8 Hz), 1.21−1.76 (m, 24H), 2.62 (t, 4H, J = 7.0 Hz), 7.67 (d, 2H, J = 9.3 Hz), 8.11 (d, 2H, J = 9.3 Hz); ^{13}C NMR (100 MHz, $CDCl_3$) δ 14.2, 20.1, 22.8, 28.8, 29.1, 29.3, 29.4, 32.0, 77.5, 102.0, 123.8, 125.1, 127.2, 131.1, 133.3; EI-MS (70 eV) m/z = 558 (M^+); Anal. Calcd for $C_{30}H_{38}Br_2$: C,64.52; H, 6.86%. Found: C, 64.28; H, 6.84%.

2,6-Dibromo-1,5-bis(phenyletynyl)naphthalene (17c). Fifty-three percent yield. Mp 223−224 °C; ^{1}H NMR (270 MHz, $CDCl_3$) δ 7.42−7.44 (m, 6H), 7.69−7.72 (m, 4H), 7.79 (d, 2H, J = 8.9 Hz), 8.27 (d, 2H, J = 8.9 Hz); ^{13}C NMR (125 MHz, $CDCl_3$) δ 86.1, 100.1, 122.8, 123.2, 125.8, 127.8, 128.7, 129.2, 131.5, 131.9, 133.0; EI-MS (70 eV) m/z = 486 (M^+); Anal. Calcd for $C_{26}H_{14}Br_2$: C,64.23; H, 2.90%. Found: C, 64.05; H, 2.56%.

General Procedure for the Cyclization of Dibromodiethynylnaphthalene Analogues. A suspension of $Na_2S\cdot 9H_2O$ (202 mg, 0.84 mmol) in NMP (6 mL) was stirred for 15 min at room temperature. The mixture was added dibromodiethynylnaphthalene analogue (0.2 mmol), and was heated at 185 °C. After the mixture was stirred for 12 h at the same temperature, the resulting mixture was added into saturated aqueous ammonium chloride (20 mL). The resulting precipitate was collected by filtration and washed with water, methanol and hexane. The residue was purified by vacuum sublimation to give naphthodithiophene derivative as a pale yellow solid.

Naphtho[2,3-*b*:6,7-*b*′]dithiophene (1a). Eighty-five percent yield. Mp > 300 °C; ^{1}H NMR (270 MHz, $CDCl_3$) δ 7.43 (d, J = 5.8 Hz, 2H), 7.51 (d, J = 5.8 Hz, 2H), 8.41 (s, 2H), 8.52 (s, 2H); EI-MS (70 eV) m/z = 240 (M^+); Anal. Calcd for $C_{14}H_8S_2$: C,69.96; H, 3.35%. Found: C, 69.76; H, 2.99%.

2,7-Dioctylnaphtho[2,3-*b*:6,7-*b*′]dithiophene (1b). Seventy-eight percent yield. Mp 269−271 °C; ^{1}H NMR (400 MHz, $CDCl_3$) δ 0.89 (t, J = 7.4 Hz, 6H), 1.28−1.50 (m, 20H), 1.75−1.83 (m, 4H), 2.92 (t, J = 7.4 Hz, 4H), 7.06 (s, 2H), 8.16 (s, 2H), 8.32 (s, 2H); EI-MS (70 eV) m/z = 464 (M^+); Anal. Calcd for $C_{30}H_{40}S_2$: C,77.53; H, 8.67%. Found: C, 77.48; H, 8.46%.

2,7-Diphenylnaphtho[2,3-*b*:6,7-*b*′]dithiophene (1c). Eighty-six percent yield. Mp > 300 °C; EI-MS (70 eV) m/z = 392 (M^+); Anal. Calcd for $C_{26}H_{16}S_2$: C,79.55; H, 4.11%. Found: C, 79.55; H, 3.90%.

Naphtho[2,3-*b*:7,6-*b*′]dithiophene (2a). Sixty-eight percent yield. Mp >300 °C; ^{1}H NMR (270 MHz, $CDCl_3$) δ 7.43 (d, J = 5.5 Hz, 2H), 7.50 (d, J = 5.5 Hz, 2H), 8.45 (s, 2H), 8.47 (s, 2H); EI-MS (70 eV) m/z = 240 (M^+); Anal. Calcd for $C_{14}H_8S_2$: C,69.96; H, 3.35%. Found: C, 69.77; H, 3.15%.

2,7-Dioctylnaphtho[2,3-*b*:7,6-*b*′]dithiophene (2b). Ninety-five percent yield. Mp 240−241 °C; ^{1}H NMR (400 MHz, $CDCl_3$) δ 0.88 (t, J = 7.0 Hz, 6H), 1.28−1.81 (m, 24H), 2.92 (t, J = 7.3 Hz, 4H), 7.05 (s, 2H), 8.21 (s, 2H), 8.26 (s, 2H); EI-MS (70 eV) m/z = 464 (M^+); Anal. Calcd for $C_{30}H_{40}S_2$: C,77.53; H, 8.67%. Found: C, 77.32; H, 8.69%.

2,7-Diphenylnaphtho[2,3-*b*:7,6-*b*′]dithiophene (2c). Seventy-one percent yield. Mp >300 °C; EI-MS (70 eV) m/z = 392 (M^+); Anal. Calcd for $C_{26}H_{16}S_2$: C,79.55; H, 4.11%. Found: C, 79.32; H, 4.15%.

Naphtho[2,1-*b*:6,5-*b*′]dithiophene (4a). Sixty percent yield. Mp 274−275 °C; ^{1}H NMR (270 MHz, $CDCl_3$) δ 7.43 (d, 2H, J = 5.4 Hz), 8.05 (d, 2H, J = 5.5 Hz), 8.05 (d, 2H, J = 8.9 Hz), 8.30 (d, 2H, J = 8.9 Hz); ^{13}C NMR (125 MHz, $CDCl_3$) δ 120.9, 121.2, 122.4, 126.4, 126.7, 136.8, 137.0; EI-MS (70 eV) m/z = 240 (M^+); Anal. Calcd for $C_{14}H_8S_2$: C,69.96; H, 3.35%. Found: C, 70.10; H, 2.95%.

2,7-Dioctylnaphtho[2,1-*b*:6,5-*b*′]dithiophene (4b). Sixty-seven percent yield. Mp 154−155 °C; ^{1}H NMR (270 MHz, $CDCl_3$) δ 0.89 (t, 6H, J = 6.8 Hz), 1.21−1.76 (m, 24H), 2.62 (t, 4H, J = 7.0 Hz), 7.67 (d, 2H, J = 9.3 Hz), 8.11 (d, 2H, J = 9.3 Hz); ^{13}C NMR (125 MHz, $CDCl_3$) δ 14.3, 22.8, 29.4, 29.4, 29.5, 31.1, 31.7, 32.0, 119.2, 119.9, 120.7, 126.3, 135.8, 137.0, 147.1; EI-MS (70 eV) m/z = 464 (M^+); Anal. Calcd for $C_{30}H_{40}S_2$: C,77.53; H, 8.67%. Found: C, 77.64; H, 8.85%.

2,7-Diphenylnaphtho[2,1-*b*:6,5-*b*′]dithiophene (4c). Fifty-six percent yield. Mp >300 °C; ^{1}H NMR (400 MHz, $CDCl_3$) δ 7.39−7.40 (m, 2H), 7.47−7.51 (m, 4H), 7.82−7.84 (m, 4H), 8.01 (d, 2H, J = 8.6 Hz), 7.71 (s, 2H), 8.05 (d, 2H, J = 8.6 Hz); EI-MS (70 eV) m/z = 392 (M^+); Anal. Calcd for $C_{26}H_{16}S_2$: C,79.55; H, 4.11%. Found: C, 79.31; H, 3.73%.

Single Crystal X-Ray Analysis. Single crystals of **1c** and **4c** suitable for X-ray structural analysis were obtained by careful recrystallization from chlorobenzene. The X-ray crystal structure analyses were made on a Rigaku Mercury-CCD (Mo Kα radiation, λ = 0.71069 Å, graphite monochromator, T = 296 K, $2\theta_{max}$ = 55.0°). The structure was solved by the direct methods.[33] Non-hydrogen atoms were refined anisotropically, and hydrogen atoms were included in the calculations but not refined. All calculations were performed using the crystallographic software package TeXsan 1.2.[34]

Crystallographic data for **1c**: $C_{26}H_{16}S_2$ (392.53), yellow plate, 0.60 × 0.50 × 0.10 mm^3, *monoclinic*, space group, $P2_1/n$ (#14), a = 5.922(10), b = 7.60(1), c = 40.63(7) Å, β = 93.753(6)°, V = 1825(5) Å^3, Z = 4, R = 0.0949 for 2229 observed reflections ($I > 2\sigma(I)$) and 253 variable parameters, wR^2 = 0.3005 for all data.

Crystallographic data for **4c**: $C_{26}H_{16}S_2$ (392.53), colorless plate, 1.0 × 0.20 × 0.05 mm^3, *monoclinic*, space group, $P2_1/c$ (#14), a = 9.517(1), b = 5.8072(8), c = 16.988(2) Å, β = 90.954(6)°, V = 938.8(2) Å^3, Z = 2, R = 0.0657 for 1563 observed reflections ($I > 2\sigma(I)$) and 127 variable parameters, wR^2 = 0.2223 for all data.

The X-ray crystal structure analysis of DPh-BTBT was made on a Rigaku DSC imaging plate system by using Si-monochromated synchrotron (λ = 1.00000 Å) at beamline BL-8B of Photon Factory (PF), High Energy Accelerator Research Organization (KEK). Crystallographic data for DPh-BTBT: Crystallographic data for DPh-BTBT: $C_{26}H_{16}S_2$ (392.53), colorless plate, 0.10 × 0.10 × 0.01 mm^3, *monoclinic*, space group, $P2_1/c$ (#14), a = 6.334(2), b = 7.462(5), c = 19.516(2) Å, β = 93.06(3)°, V = 921.1(7) Å^3, Z = 2, R = 0.0843 for 1284 observed reflections ($I > 2\sigma(I)$) and 152 variable parameters, wR^2 = 0.2377 for all data.

Fabrication and Evaluation of FET Devices. OFETs were fabricated in a "top-contact" configuration on a heavily doped n^+-Si (100) wafer with a 200 nm thermally grown SiO_2 (C_i = 17.3 nF cm^{-2}). The substrate surfaces were treated with octyltrichlorosilane (OTS) or hexamethyldisilazane (HMDS) as reported previously.[3d] A thin film NDT derivatives as the active layer was vacuum-deposited on the Si/SiO_2 substrates maintained at various temperatures (T_{sub}) at a rate of 1 Å s^{-1} under a pressure of ~10^{-3} Pa. On top of the organic thin film, gold films (80 nm) as drain and source electrodes were deposited through a shadow mask. For a typical device, the drain-source channel length (L) and width (W) are 50 μm and 1.5 mm, respectively. Characteristics of the OFET devices were measured at room temperature under ambient conditions with a Keithley 4200 semiconducting parameter analyzer. Field-effect mobility (μ_{FET}) was calculated in the saturation (V_d = −60 V) or linear regime (V_d = −5 V) of the I_d using the following equation,

$$\text{Saturation regime}: I_d = C_i\mu_{FET}(W/2L)(V_g - V_{th})^2$$

$$\text{Linear regime}: I_d = V_d C_i \mu_{FET}(W/L)(V_g - V_{th})$$

where C_i is the capacitance of the SiO_2 insulator, and V_g and V_{th} are the gate and threshold voltages, respectively. Current on/off ratio (I_{on}/I_{off}) was determined from the I_d at V_g = 0 V (I_{off}) and V_g = −60 V (I_{on}). The μ_{FET} data reported are typical values from more than ten different devices.

■ ASSOCIATED CONTENT

Supporting Information. Instrumentation for the characterization of compounds and physicochemical evaluation, repeated voltammograms of **1a**−**4a**, absorption spectra of **1a** and naphthacene in air saturated solution, crystal structure of **3c**, simulated powder patterns from the bulk single crystal structures of **1c** and DPh-BTBT, shelf-life time test of **1c**-based FET, calculated transfer integrals (t) of **3c** and **4c** based on the bulk-single crystal structures, results on TD-DFT calculations of **1a**−**4a**, AFM images of evaporated thin film of **1c**, **2c** (T_{sub} = rt), and **4c** (T_{sub} = 100 °C), complete ref 20, NMR spectra of compounds, crystallographic information file (CIF) for **1c**, **4c** and DPh-BTBT. This material is available free of charge via the Internet at http://pubs.acs.org.

■ AUTHOR INFORMATION

Corresponding Author
ktakimi@hiroshima-u.ac.jp

■ ACKNOWLEDGMENT

This work was partially supported by a Grant-in-Aid for Scientific Research (No. 20350088) from the Ministry of Education, Culture, Sports, Science and Technology, Japan and The Strategic Promotion of Innovative Research and Development from the Japan Science and Technology Agency. Combustion elemental analyses were carried out at the Natural Science Center for Basic Research and Development (N-BARD), Hiroshima University.

■ REFERENCES

(1) (a) Laquindanum, J. G.; Katz, H. E.; Lovinger, A. J.; Dodabalapur, A. *Adv. Mater.* **1997**, *8*, 36–39. (b) Takimiya, K.; Kunugi, Y.; Konda, Y.; Niihara, N.; Otsubo, T. *J. Am. Chem. Soc.* **2004**, *126*, 5084–5085. (d) Takimiya, K.; Kunugi, Y.; Ebata, H.; Otsubo, T. *Chem. Lett.* **2006**, *35*, 1200–1201. (e) Kashiki, T.; Miyazaki, E.; Takimiya, K. *Chem. Lett.* **2008**, *37*, 284–285. (f) Kashiki, T.; Miyazaki, E.; Takimiya, K. *Chem. Lett.* **2009**, *38*, 568–569.

(2) (a) Laquindanum, J. G.; Katz, H. E.; Lovinger, A. J. *J. Am. Chem. Soc.* **1998**, *120*, 664–672. (b) Payne, M. M.; Parkin, S. R.; Anthony, J. E.; Kuo, C.-C.; Jackson, T. N. *J. Am. Chem. Soc.* **2005**, *127*, 4986–4987. (c) Dickey, K. C.; Anthony, J. E.; Loo, Y. L. *Adv. Mater.* **2006**, *18*, 1721–1726. (d) Chen, M.-C.; Kim, C.; Chen, S.-Y.; Chiang, Y.-J.; Chung, M.-C.; Facchetti, A.; Marks, T. J. *J. Mater. Chem.* **2008**, *18*, 1029–1036.

(3) (a) Li, X. -C.; Sirringhaus, H.; Garnier, F.; Holmes, A. B.; Moratti, S. C.; Feeder, N.; Clegg, W.; Teat, S. J.; Friend, R. H. *J. Am. Chem. Soc.* **1998**, *120*, 2206–2207. (b) Sirringhaus, H.; Friend, R. H.; Wang, C.; Leuninger, J.; Mullen, K. *J. Mater. Chem.* **1999**, *9*, 2095–2101. (c) Anthony, J. E. *Chem. Rev.* **2006**, *106*, 5028–5048. (d) Takimiya, K.; Ebata, H.; Sakamoto, K.; Izawa, T.; Otsubo, T.; Kunugi, Y. *J. Am. Chem. Soc.* **2006**, *128*, 12604–12605. (e) Takimiya, K.; Kunugi, Y.; Konda, Y.; Ebata, H.; Toyoshima, Y.; Otsubo, T. *J. Am. Chem. Soc.* **2006**, *128*, 3044–3050. (f) Yamamoto, T.; Takimiya, K. *J. Am. Chem. Soc.* **2007**, *129*, 2224–2225. (g) Ebata, H.; Izawa, T.; Miyazaki, E.; Takimiya, K.; Ikeda, M.; Kuwabara, H.; Yui, T. *J. Am. Chem. Soc.* **2007**, *129*, 15732–15733. (h) Takimiya, K.; Kunugi, Y.; Otsubo, T. *Chem. Lett.* **2007**, *36*, 578–583. (i) Gao, J.; Li, R.; Li, L.; Meng, Q.; Jiang, H.; Li, H.; Hu, W. *Adv. Mater.* **2007**, *19*, 3008–3011. (j) Anthony, J. E. *Angew. Chem., Int. Ed.* **2008**, *47*, 452–483. (k) Izawa, T.; Miyazaki, E.; Takimiya, K. *Adv. Mater.* **2008**, *20*, 3388–3392. (l) Gao, P.; Beckmann, D.; Tsao, H. N.; Feng, X.; Enkelmann, V.; Baumgarten, M.; Pisula, W.; Müllen, K. *Adv. Mater.* **2009**, *21*, 213–216.

(4) (a) Pan, H.; Li, Y.; Wu, Y.; Liu, P.; Ong, B. S.; Zhu, S.; Xu, G. *Chem. Mater.* **2006**, *18*, 3237–3241. (b) Pan, H.; Li, Y.; Wu, Y.; Liu, P.; Ong, B. S.; Zhu, S.; Xu, G. *J. Am. Chem. Soc.* **2007**, *129*, 4112–4113. (c) Pan, H.; Wu, Y.; Li, Y.; Liu, P.; Ong, B. S.; Zhu, S.; Xu, G. *Adv. Funct. Mater.* **2007**, *17*, 3574–3579.

(5) (a) Liang, Y.; Wu, Y.; Feng, D.; Tsai, S.-T.; Son, H.-J.; Li, G.; Yu, L. *J. Am. Chem. Soc.* **2009**, *131*, 56–57. (b) Liang, Y.; Feng, D.; Wu, Y.; Tsai, S.-T.; Li, G.; Ray, C.; Yu, L. *J. Am. Chem. Soc.* **2009**, *131*, 7792–7799. (c) Huo, L.; Hou, J.; Zhang, S.; Chen, H. Y.; Yang, Y. *Angew. Chem. Inter. Ed.* **2010**, *49*, 1500–1503. (d) Liang, Y.; Xu, Z.; Xia, J.; Tsai, S.-T.; Wu, Y.; Li, G.; Ray, C.; Yu, L. *Adv. Mater.* **2010**, *22*, E135–E138. (e) Piliego, C.; Holcombe, T. W.; Douglas, J. D.; Woo, C. H.; Beaujuge, P. M.; Fréchet, J. M. *J. Am. Chem. Soc.* **2010**, *132*, 7595–7597. (f) Zhang, Y.; Hau, S. K.; Yip, H.-L.; Sun, Y.; Acton, O.; Jen, A. K. Y. *Chem. Mater.* **2010**, *22*, 2696–2698. (g) Zou, Y.; Najari, A.; Berrouard, P.; Beaupré, S.; Aïch, B. R.; Tao, Y.; Leclerc, M. J., M. *J. Am. Chem. Soc.* **2010**, *132*, 5330–5331.

(6) Lloyd, M. T.; Mayer, A. C.; Subramanian, S.; Mourey, D. A.; Herman, D. J.; Bapat, A. V.; Anthony, J. E.; Malliaras, G. G. *J. Am. Chem. Soc.* **2007**, *129*, 9144–9149.

(7) (a) Mühlbacher, D.; Scharber, M.; Morana, M.; Zhu, Z.; Waller, D.; Gaudiana, R.; Brabec, C. *Adv. Mater.* **2006**, *18*, 2884–2889. (b) Hou, J.; Chen, H.-Y.; Zhang, S.; Li, G.; Yang, Y. *J. Am. Chem. Soc.* **2008**, *130*, 16144–16145.

(8) (a) Wang, C.-H.; Hu, R.-R.; Liang, S.; Chen, J.-H.; Yang, Z.; Pei, J. *Tetrahedron Lett.* **2005**, *46*, 8153–8157. (b) Ebata, H.; Miyazaki, E.; Yamamoto, T.; Takimiya, K. *Org. Lett.* **2007**, *9*, 4499–4502. (c) Zhou, Y.; Liu, W.-J.; Ma, Y.; Wang, H.; Qi, L.; Cao, Y.; Wang, J.; Pei, J. *J. Am. Chem. Soc.* **2007**, *129*, 12386–12387.

(9) (a) Beimling, P.; Koβmehl, G. *Chem. Ber.* **1986**, *119*, 3198–3203. (b) Takimiya, K.; Konda, Y.; Ebata, H.; Niihara, N.; Otsubo, T. *J. Org. Chem.* **2005**, *70*, 10569–10571. (c) Kashiki, T.; Shinamura, S.; Kohara, M.; Miyazaki, E.; Takimiya, K.; Ikeda, M.; Kuwabara, H. *Org. Lett.* **2009**, *11*, 2473–2475.

(10) Coropceanu, V.; Kwon, O.; Wex, B.; Kaafarani, B. R.; Gruhn, N. E.; Durivage, J. C.; Neckers, D. C.; Bredas, J.-L. *Chem.—Eur. J.* **2006**, *12*, 2073–2080.

(11) (a) Umeda, R.; Fukuda, H.; Miki, K.; Rahman, S. M. A.; Sonoda, M.; Tobe, Y. *C. R. Chimie* **2009**, *12* 378−384. see also (b) Tilak, B. D. *Proc. Indian Acad. Sci. Sect. A* **1951**, *33A*, 71–77.

(12) Shinamura, S.; Miyazaki, E.; Takimiya, K. *J. Org. Chem.* **2010**, *75*, 1228–1234.

(13) Osaka, I.; Abe, T.; Shinamura, S.; Miyazaki, E.; Takimiya, K. *J. Am. Chem. Soc.* **2010**, *132*, 5000–5001.

(14) Mataka, S.; Takahashi, K.; Ikezaki, Y.; Hatta, T.; Tori-i, A.; Tashiro, M. *Bull. Chem. Soc. Jpn.* **1991**, *64*, 68–73.

(15) (a) Cooke, R. G.; Johnson, B. L.; Owen, W. R. *Aust. J. Chem.* **1960**, *13*, 256–260. (b) Kitamura, C.; Ohara, T.; Kawatsuki, N.; Yoneda, A.; Kobayashi, T.; Naito, H.; Komatsu, T.; Kitamura, T. *CrystEngComm* **2007**, *9*, 644–647.

(16) Wheeler, A. S.; Ergle, D. R. *J. Am. Chem. Soc.* **1930**, *52*, 4872–4880.

(17) Wheeler, A. S.; Mattox, W. J. *J. Am. Chem. Soc.* **1933**, *55*, 686–690.

(18) Takimiya, K.; Yamamoto, T.; Ebata, H.; Izawa, T. *Sci. Tech. Adv. Mater.* **2007**, *8*, 273–276.

(19) (a) Suresh, C. H.; Gadre, S. R. *J. Org. Chem.* **1999**, *64*, 2505–2512. (b) Poater, J.; Visser, R.; Sola, M.; Bickelhaupt, F. M. *J. Org. Chem.* **2007**, *72*, 1134–1142.

(20) MO calculations were carried out with the DFT/TD-DFT method at the B3LYP/6-31g(d) level using Gaussian 03 program package. Frisch, M. J. et al. *Gaussian 03*, revision C.02; Gaussian, Inc.: Wallingford, CT, 2004.

(21) Maliakal, A.; Raghavachari, K.; Katz, H.; Chandross, E.; Siegrist, T. *Chem. Mater.* **2004**, *16*, 4980–4986.

(22) (a) Tang, M. L.; Okamoto, T.; Bao, Z. *J. Am. Chem. Soc.* **2006**, *128*, 16002–16003. (b) Valiyev, F.; Hu, W.-S.; Chen, H.-Y.; Kuo, M.-Y.; Chao, I.; Tao, Y.-T. *Chem. Mater.* **2007**, *19*, 3018–3026. (c) Tang, M. L.; Mannsfeld, S. C. B.; Sun, Y.-S.; Becerril, H. t. A.; Bao, Z. *J. Am. Chem. Soc.* **2009**, *131*, 882–883.

(23) Takimiya, K.; Kunugi, Y.; Toyoshima, Y.; Otsubo, T. *J. Am. Chem. Soc.* **2005**, *127*, 3605–3612.

(24) ADF2008.01. SCM *Theoretical Chemistry*; Vrije Universiteit: Amsterdam, The Netherlands, http://www.scm.com.

(25) (a) Senthilkumar, K.; Grozema, F. C.; Bickelhaupt, F. M.; Siebbeles, L. D. A. *J. Chem. Phys.* **2003**, *119*, 9809–9817. (b) Prins, P.; Senthilkumar, K.; Grozema, F. C.; Jonkheijm, P.; Schenning, A. P. H. J.; Meijer, E. W.; Siebbeles, L. D. A. *J. Chem. Phys. B* **2005**, *109*, 18267–18274.

(26) (a) Valiyev, F.; Hu, W.-S.; Chen, H.-Y.; Kuo, M.-Y.; Chao, I.; Tao, Y.-T. *Chem. Mater.* **2007**, *19*, 3018–3026. (b) Kim, E.-G.; Coropceanu, V.; Gruhn, N. E.; Sanchez-Carrera, R. S.; Snoeberger, R.; Matzger, A. J.; Bredas, J.-L. *J. Am. Chem. Soc.* **2007**, *129*, 13072–13081.

(27) These transfer integrals are also larger than those calculated for **3c** (∼25 meV) and **4c** (∼11 meV) using the bulk single crystal structures. See Supporting Information.

(28) Sanchez-Carrera, R. S.; Atahan, S.; Schrier, J.; Aspuru-Guzik, A. *J. Phys. Chem. C* **2010**, *114*, 2334–2340.

(29) (a) Bredas, J.-L.; Beljonne, D.; Coropceanu, V.; Cornil, J. *Chem. Rev.* **2004**, *104*, 4971–5004. (b) Sakanoue, K.; Motoda, M.; Sugimoto, M.; Sakaki, S. *J. Chem. Phys. A* **1999**, *103*, 5551–5556.

(30) λ^hs for **2a**−**4a** are 100, 266, and 245 meV, respectively, reflecting their electronic structures.

(31) (a) Kano, M.; Minari, T.; Tsukagoshi, K. *Appl. Phys. Lett.* **2009**, *94*, 143304. (b) Kobayashi, N.; Sasaki, M.; Nomoto, K. *Chem. Mater.* **2009**, *21*, 552–556.

(32) Meng, H.; Bao, Z.; Lovinger, A. J.; Wang, B.-C.; Mujsce, A. M. *J. Am. Chem. Soc.* **2001**, *123*, 9214–9215.

(33) Sheldrick, G. M. *SHELXL (SHELX97)*. Programs for the refinement of crystal structures. University of Goettingen: Germany, 1997.

(34) *teXsan: Single Crystal Structure Analysis Software*, Version 1.19; Molecular Structure Corporation and Rigaku Corporation: 2000.